The Dynamics of Northern Hemisphere Stratospheric Final Warming Events

Robert X. Black
Brent A. McDaniel
School of Earth and Atmospheric Sciences
Georgia Institute of Technology
Atlanta, Georgia

November 2006
(To appear in the *Journal of the Atmospheric Sciences:*
Special Issue on Annular Modes and Jets)

Corresponding author address:
Dr. Robert X. Black
School of Earth and Atmospheric Sciences
Georgia Institute of Technology
Atlanta, GA 30332-0340
E-mail: rob.black@eas.gatech.edu

ABSTRACT

A lag composite analysis is performed of the zonal-mean structure and dynamics of Northern Hemisphere stratospheric final warming (SFW) events. SFW events are linked to distinct zonal wind deceleration signatures in the stratosphere and troposphere. The period of strongest stratospheric decelerations (SD) is marked by a concomitant reduction in the high latitude tropospheric westerlies. However, a subsequent period of tropospheric decelerations (TD) occurs while the stratospheric circulation relaxes toward climatological conditions. During SFW onset a wavenumber one disturbance at stratospheric altitudes evolves into a circumpolar anticyclonic circulation anomaly.

Transformed Eulerian-Mean dynamical diagnoses reveal that the SD period is characterized by an anomalous upward Eliassen-Palm (E-P) signature at high latitudes extending from the surface to the middle stratosphere. The associated wave driving pattern consists of zonal decelerations extending from the upper troposphere to the mid-stratosphere. Piecewise potential vorticity tendency analyses further indicate that zonal wind decelerations in the lower and middle troposphere result, at least in part, from the direct response to latitudinal redistributions of potential vorticity occurring in the lower stratosphere. The TD period exhibits a distinct dynamical behavior with anomalous downward E-P fluxes in the high latitude stratosphere as the zero zonal wind line descends toward the tropopause. This simultaneously allows the stratospheric polar vortex to radiatively recover while providing anomalous upper tropospheric zonal decelerations (as tropospheric Rossby wave activity is vertically trapped in the high latitude troposphere). The tropospheric decelerations that occur during the TD period are regarded as a subsequent indirect consequence of SFW events.

1. Introduction

The extratropical stratosphere exhibits a pronounced annual cycle in which the large-scale circulation ranges from strong circumpolar westerlies (the stratospheric polar vortex) during winter to weaker circumpolar easterlies during summer (Andrews et al. 1987). The wintertime polar vortex exhibits considerable variability on interannual and intraseasonal time scales. Subseasonal polar vortex weakenings during winter are known as sudden stratospheric warmings (SSWs), and each winter terminates with a relatively rapid breakdown of the polar vortex known as the stratospheric final warming (SFW), marking the final transition from westerlies to easterlies in the extratropical stratosphere. There is considerable interannual variability in the timing of SFW events (Waugh and Rong 2002) since they are sensitive to the preexisting stratospheric flow structure and variations in the upward propagation of tropospheric planetary waves (Waugh et al. 1999). SFW events are more frequent than SSW events, which occur at a frequency of 0.6 events per year (Charlton and Polvani, 2006, CP hereafter).

Circumpolar (annular) variability in the Northern Hemisphere circulation provides a strong link between the winter stratospheric polar vortex and tropospheric climate (Thompson and Wallace 2000, Baldwin and Dunkerton 2001, Thompson et al. 2005). In particular, the polar vortex strength is strongly connected to the Northern Annular Mode (NAM) and anomalous tropospheric weather conditions (Thompson and Wallace 2001, Baldwin et al. 2003). Also, polar vortex variations have been linked to regional variability in column ozone and incoming UV flux at the Earth's surface (Karpetchko et al 2005). Although annular modes occur over a wide range of time scales (weeks to decades), there has been a substantial focus on subseasonal variability (e.g., Limpasuvan et al. 2004, McDaniel and Black 2005, hereafter MB) and long-term trends (Thompson and Solomon 2002, Gillett and Thompson 2003). The past studies of subseasonal NAM variability encompass

SSW events and their connection to the NAM (Limpasuvan et al. 2004).

The recent observational analysis of Black et al. (2006, BMR hereafter) examined some of the basic phenomenological aspects of boreal stratospheric final warming events. BMR find that SFW events strongly organize the large-scale circulation of the stratosphere and troposphere during the period of spring onset. In contrast to the climatological seasonal cycle, SFW events accelerate the annual weakening of high latitude circumpolar westerlies simultaneously at stratospheric and tropospheric altitudes. This behavior is manifested by a coherent pattern of westerly (easterly) annular zonal wind anomalies extending from the mid-stratosphere to the Earth's surface at high latitudes prior to (after) SFW events, coinciding with the polar vortex breakdown.

BMR's results suggest that SFW events are associated with a robust large-scale coupling of the stratosphere and troposphere with a distinct regional circulation change in the lower troposphere, consisting of geopotential height rises over polar latitudes and height falls over the northeast North Atlantic. Although some parallels do exist, an important result is that the circulation structures identified in association with SFW events are structurally distinct from the canonical NAM (and SSW) patterns. A primary difference is that the major extratropical anomaly features are retracted and/or shifted northward toward the pole in comparison to the NAM. As a consequence, the near-surface anomaly patterns identified in BMR do not correspond very well to the Arctic Oscillation (the surface manifestation of the NAM). Thus, from a synoptic perspective, SFW events have important distinctions from SSW events.

Another interesting aspect of the tropospheric response to SFW events found by BMR is that the tropospheric annular evolution is comprised of two distinct deceleration periods: In the 10 days prior to SFW onset (Day 0), the period of strongest stratospheric decelerations, the tropospheric and

stratospheric zonal winds decelerate simultaneously. However, there is also a second tropospheric deceleration period, between Days +5 and +10, during which time the stratospheric zonal wind field generally accelerates, relaxing toward climatological conditions. In fact, it is the second deceleration period that leads to the largest amplitude tropospheric zonal wind anomalies after SFW onset. BMR speculate that the first and second tropospheric deceleration periods, respectively, are associated with direct and indirect tropospheric responses to changes in the lower stratospheric circulation (e.g., see discussion in MB). As such, SFW events provide an excellent phenomenological basis for testing existing theoretical ideas on stratosphere-troposphere dynamical coupling.

In order to address this question we extend BMR's phenomologically-oriented study with a dynamically-oriented analysis of the composite zonal-mean evolution of SFW events. Our primary goal is to infer the basic physical mechanisms responsible for tropospheric zonal flow decelerations occurring in association with SFW events. In approaching this problem we first characterize the time evolution of the composite annular circulation and stratospheric wave patterns during SFW events. This includes an analysis of the high latitude potential vorticity anomaly evolution. We then perform dynamical analyses for the two tropospheric deceleration periods discussed above. A transformed Eulerian mean analysis is performed to assess the impact of large-scale Rossby waves upon the time evolution of the tropospheric and stratospheric zonal flow. We also perform parallel piecewise potential vorticity tendency analyses to test for possible stratospheric feedbacks on the tropospheric zonal flow field. We do not perform an a priori projection of the data upon predetermined modes of variability (such as the NAM). Section 2 outlines our approach, the SFW structural and dynamical analyses are presented in Sections 3 and 4, respectively, and Section 5 provides concluding remarks.

2. Data and Methods

Our study employs 47 years (1958-2004) of National Centers for Environmental Prediction/ National Center for Atmospheric Research (NCEP-NCAR) daily-average reanalyses (Kalnay et al. 1996) archived on 17 pressure levels extending from 1000 hPa to 10 hPa. We consider both total and anomaly fields, where the latter are defined as deviations from a smoothed climatological seasonal march (itself defined as the sum of the first 6 Fourier harmonics of a seasonal cycle derived from an annual time-series of long-term daily averages).

Following BMR, we are interested in constructing composites relative to the time when SFW events emerge in the lower stratosphere (when tropospheric linkages are expected to be maximized). As such, SFW events are identified as the final time that the 50 hPa zonal-mean zonal wind at 70°N (the core latitude of the stratospheric polar vortex) drops below zero without returning to a specified positive threshold value (5 m/s) until the subsequent autumn. Further details on the identification procedure are outlined in BMR. Applying this criterion to running 5-day averages, we determine that SFW onset usually occurs between mid-March and late May with a mean onset date of April 14. As discussed in BMR, our procedure isolates a late stage in the polar vortex breakdown characterized by the onset of easterlies within the vortex core. The SFW dates identified are then used to construct a lag composite evolution of the 47 individual events (Day 0 denotes SFW onset). The statistical significance of composite anomalies is assessed using a Student t-test (in which each annual SFW event is considered an independent sample) and here we restrict our attention to significant features.

We employ two of the dynamical diagnostic tools used by MB in their study of subseasonal variability in the NAM. First, the transformed Eulerian mean (TEM) dynamical framework is used

to study the net eddy-forcing (wave driving) of the zonal mean flow. The quasi-geostrophic (QG) form of the TEM zonal mean momentum equation is given by:

$$\frac{\partial \overline{u}}{\partial t} = f\,\overline{v}_r + \frac{e^{z/H}}{r\cos\phi}\nabla \cdot \underset{\sim}{F} + D_x \qquad (1)$$

where $\overline{u}$ is the zonally-averaged zonal wind, f is the Coriolis parameter, $\overline{v}_r$ is the residual mean meridional velocity, z is a log-pressure coordinate with scale height H, ϕ is latitude, r is the radius of the Earth, D_x is a frictional dissipation, and $\underset{\sim}{F}$ is the Eliassen-Palm (EP) flux (Palmer 1981). Equation (1) is applied in the following way: Composite zonal wind anomaly tendencies (LHS) are studied in relation to composite anomalies in the EP flux and wave driving (second term on RHS) over specific time periods of interest. Our analysis implicitly includes the net impact of anomalies in both the propagating and quasi-stationary wave field. We are particularly interested in studying the two tropospheric deceleration periods discussed in the Introduction.

As discussed by MB, EP fluxes provide a direct measure of Rossby-wave propagation in the meridional plane (Edmon et al. 1980). Further, the EP flux divergence is directly proportional to both the (i) meridional eddy flux of potential vorticity and (ii) net wave driving of the zonal-mean zonal wind (equations 3.5.10 and 3.5.2, respectively, of Andrews et al. 1987). We note that, for nonzero tendencies, equation (1) embodies a crucial dynamical interplay between the mechanical wave driving and Coriolis torque. Specifically, as wave driving locally accelerates/decelerates the zonal wind field, a residual mean secondary circulation is induced in such a manner to restore thermal wind balance. The end result is an effective vertical "spreading" of the zonal wind response (e.g., see Fig 12.11 of Holton 2004).

In principal, this vertical spreading can extend across the tropopause. To quantify this effect, piecewise potential vorticity (PV) inversions are performed to infer the extent to which wave driving (via its impact on the meridional distribution of potential vorticity) within each domain (troposphere or stratosphere) acts to modify the zonal flow. First the zonal-mean distribution of PV anomalies is calculated. Then, individual PV "pieces" are inverted to assess the remote circulations associated with localized PV structures (e.g, Davis 1992). Using the piecewise PV inversion approach, one can assess the role of stratospheric PV anomalies in the formation of tropospheric zonal wind anomalies and vice-versa. We note that positive (negative) PV anomalies in the high latitude stratosphere will be associated with circumpolar westerly (easterly) zonal wind anomalies to the south (Black 2002). The piecewise PV inversion procedure that we employ follows MB in that piecewise PV tendency inversions are performed. In this case the *time derivative* of the zonal-mean PV field is assessed and specific features in the PV-tendency field are inverted. This yields the annular zonal-wind tendency induced by the specific zonal-mean PV-tendency feature under consideration. We can then attribute localized changes in the zonal-mean zonal wind field separately to tropospheric and stratospheric redistributions of PV. The piecewise PV tendency inversions thereby provide a diagnostic means for inferring the residual feedback of stratospheric dynamical processes upon the tropospheric zonal wind tendencies. Further details and discussion of the piecewise PV tendency procedure can be found in MB. Taken together, the TEM and piecewise PV tendency analyses provide inferences on the underlying physical mechanisms responsible for the annular zonal flow decelerations that are associated with SFW events.

3. Structural Evolution

We begin with an overview of the composite annular circulation evolution surrounding the time of SFW onset. The composite zonal-mean zonal wind anomalies and total zonal wind field are displayed in Figs. 1 and 2, respectively. Fifteen days prior to onset positive zonal wind anomalies are observed through much of the high latitude stratosphere and between mid to high latitudes in the troposphere. Over the next 5 days the pattern of significant tropospheric westerly anomalies spreads northward to cover latitudes north of 60°N while the stratospheric westerly anomalies retract poleward and downward. The pattern of tropospheric and stratospheric westerly anomalies weakens between days -10 and -5 while easterly anomalies emerge at high latitudes in the mid-stratosphere. Between day -5 and onset, the pattern of easterly anomalies undergoes a dramatic intensification and dives quickly downward through the lower stratosphere into the lower troposphere, replacing the pattern of westerly anomalies. It is clear that marked stratospheric and tropospheric decelerations take place between Days -10 and Day 0 within 60°N and 90°N. After onset there is a brief period during which (i) the stratospheric anomaly pattern broadens and (ii) the tropospheric anomaly pattern shifts southward. Thereafter, the stratospheric anomalies weaken while there is a second burst of zonal deceleration in the high latitude troposphere concentrated between 70°N and 80°N. It is at this time (Day +10) that the tropospheric easterly anomalies achieve peak amplitudes at high latitudes.

The parallel evolution of the total zonal wind field at high latitudes is generally consistent with the anomaly evolution. However, it is useful to note that the total wind evolution implicitly contains elements of the climatological seasonal trend. For example, evidence of this trend can be found in the vicinity of the subtropical jet stream (below the tropopause near 30°N) which weakens

by at least 5 m s^{-1} while there is little or no change in the anomaly field during this time (Fig. 1). At Day -15 westerly winds in excess of 10 m s^{-1} extend over much of the lower stratosphere at mid-latitudes. The mid to high latitude westerlies are observed to dramatically weaken and retract downward in the lower stratosphere as SFW onset approaches. Thereafter, easterlies appear in the mid-stratosphere at high latitudes with the zero wind line descending into the lower stratosphere. The strongest easterly winds are observed at Day +5 near 10 hPa. During the evolution the tropospheric subtropical jet is observed to weaken and broaden latitudinally. There are marked zonal decelerations at mid to high latitudes in the troposphere.

The high latitude zonal wind evolution is summarized in Fig. 3[1]. There are several features of interest to note. First, as discussed by BMR, we note the apparent stratospheric preconditioning that occurs 30 days prior to onset. The strongest westerly anomalies then slowly drift downward within the stratosphere between Day -30 and -10. The period between Day -10 and 0 is characterized by a dramatic and vertically coherent zonal deceleration pattern extending through the entire vertical domain. The strongest stratospheric decelerations are observed to occur during this time period (hereafter referred to as SD). Interestingly, the tropospheric easterly anomalies within this latitude band then weaken for a few days just after SFW onset. This is followed by a second tropospheric deceleration period (hereafter referred to as TD) between Days +5 and +10 leading to peak amplitude tropospheric easterly anomalies at Day +10. Curiously, the TD period is actually associated with stratospheric *accelerations* as the large-scale stratospheric circulation relaxes toward climatology. The features described above (including the SD and TD deceleration periods) are evident in the time evolution of both the anomalous (Fig. 3a) and total (Fig. 3b) zonal wind field.

[1] For reference purposes, Fig. 3a is reproduced from Fig. 3 of BMR.

It is well recognized from composite analyses that SSWs are linked to anomalous planetary wave activity emanating from tropospheric altitudes (Limpasuvan et al. 2004, CP). As such, it is of interest to here study the composite evolution of the stratospheric wave field, which is characterized via horizontal maps of both the 50 hPa (a) geopotential height field (Fig. 4) and (b) quasi-geostrophic PV anomaly field (Fig. 5) for the same time lags considered in Figs 1 and 2[2]. The geopotential height field is geostrophically linked to the *total* large-scale horizontal circulation while the PV anomaly field is qualitatively linked to circulation *anomalies*. The early composite evolution (Day -15) is associated with anomalously high PV in the eastern Arctic (Fig. 5a) with a strengthened polar vortex (consistent with the westerly zonal wind anomalies in Fig. 1a). Weak negative PV anomalies are found over northern Canada. Over the course of the next 10 days (Day -15 to Day -5), a prominent wavenumber one disturbance develops over high latitudes with positive PV anomalies over the eastern Arctic Ocean and negative anomalies over northernmost Canada[3]. This pattern promotes a strengthening and eastward displacement of the climatological Aleutian High and a southward displacement of the polar vortex (Figs. 4b-c). In the parlance of CP, the composite SFW structure is analogous to an SSW "vortex displacement" event. During SFW onset, the negative PV anomaly feature strengthens and shifts poleward consistent with the observed zonal flow deceleration (Fig. 4d). Thereafter a band of weak positive PV anomalies forms at mid-latitudes

---

[2] For visual display purposes, the PV fields are low-pass filtered using a 151-point Lanczos filter that isolates periods greater than 10 days. This reduces the "noisiness" of the PV field without altering the basic PV anomaly structures.

[3] A case by case analysis of the eddy kinetic energy spectrum reveals that wavenumber 1 power exceeds that of wavenumber 2 in 70% of the SFW events.

(Fig. 5e-f). The PV evolution indicates that SFW events lead to a net southward transport of PV, as positive polar PV anomalies are replaced by negative circumpolar anomalies.

The precursor westerly anomaly pattern observed at early stages in the SFW time evolution (Figs. 1a-1b) is stronger in amplitude and extends to considerably lower altitudes than the analogous precursor patterns found by Limpasuvan et al. (2004) in their composite study of intraseasonal SSW events. Better correspondence is found with the precursors to "vortex splitting" (wavenumber 2) events studied in the recent SSW study of CP. The post-SFW easterly anomaly patterns are retracted toward high latitudes in comparison to the post-SSW structures identified by Limpasuvan et al. (2004) and CP. In contrast to the zonal-mean results, the longitudinally varying stratospheric circulation evolution during SFW events (Fig. 4) more closely resembles the case study of "vortex displacement" displayed in Fig. 1a of CP. We note that, for SFW events, the resulting *tropospheric* easterly anomaly structures appear distinct from the canonical NAM structure, as the local zonal wind extrema are generally observed well north of 55^{o}N, the tropospheric latitudinal extremum for the NAM (Thompson and Wallace 2000). Since NAM events impact the polar vortex strength, these differences indicate that SFW events may, at least in part, be related to latitudinal shifts in the polar vortex. In summary, although there are some qualitative similarities in the composite structural evolution of SSW and SFW events, there are also notable differences.

4. Dynamical Evolution

The synoptic structural analyses of the previous section provide an ideal setting for further, more dynamically-oriented analyses of SFW evolution. We earlier noted that, considering large-scale balance conditions, annular circumpolar circulation anomalies will be associated with polar potential vorticity anomalies. We have observed that the stratospheric and tropospheric decelerations

noted in Fig. 3 are associated with concomitant changes in near-polar PV in the stratosphere (Fig. 5). This is further studied in Fig. 6 which shows the corresponding time evolution of the PV anomaly field as well as the associated PV tendency field, both averaged over the polar cap. Comparing with the zonal wind anomaly evolution displayed in Fig. 3, it is clear that the stratospheric westerly (easterly) anomalies are related to near-polar positive (negative) PV anomalies (Fig. 6a). We further note that during the period of strong stratospheric decelerations (Days -10 to 0), there is a robust matching stratospheric pattern of negative PV tendencies. This is followed by a more gradual PV increase as the polar vortex gradually returns to climatological conditions. At tropospheric altitudes it is clear that the tropospheric westerly anomaly signature at Day -10 is linked to positive PV anomalies in the upper troposphere (An analogous linkage is observed for the easterly anomaly signature observed at Day +10). The upper tropospheric PV then decreases around Day -6, prior to the above-mentioned PV decreases in the lower stratosphere. This is consistent with the idea that there is some initial absorption of the anomalous upward wave activity pulse as it crosses the tropopause. We note, however, that the relationship between the tropospheric zonal wind and PV anomaly fields around Day 0 is inconsistent (noting there are actually upper tropospheric PV *increases* at Lag 0). This raises the possibility that some of the tropospheric decelerations that occur during the SD period may, in fact, arise from PV changes occurring in the lower stratosphere (noting the strong vertical coherence of the zonal wind deceleration occurring just prior to Day 0). This is directly addressed in the subsequent analyses.

Given the relatively short time scales for the stratospheric PV decreases observed just prior to SFW onset (in comparison to lower stratospheric radiative and dissipative time scales, typically $\gtrsim$ 15 days), these PV changes are most likely the consequence of meridional transports of PV by

planetary-scale eddies. We recall that the meridional eddy flux of PV is directly proportional to the wave driving term in equation (1) (which itself is proportional to the EP flux divergence). Thus, we would anticipate that the near-polar stratospheric PV decreases observed during the SD period in Fig. 6 should be associated with a large-scale pattern of negative wave driving anomalies (and southward eddy PV fluxes) having maximum amplitudes at sub-polar latitudes. The analyses presented in Fig. 7 confirm that this is, indeed, the case.

Fig. 7 displays dynamical tendency analyses for the SD period (Days -10 to 0). The mean zonal wind tendency during this period (Fig. 7a) consists of a vertically coherent pattern of zonal decelerations extending over stratospheric and tropospheric altitudes between 60^{o}N and 90^{o}N, with strongest decelerations in the mid to lower stratosphere. Considerably weaker zonal accelerations are observed at lower latitudes in the stratosphere. A corresponding analysis of the EP flux and wave driving anomalies (Fig. 7b) reveals a prominent upwards EP flux anomaly pattern extending from the Earth's surface to the mid-stratosphere. There are associated large-scale patterns of negative wave driving (anomalous EP flux convergence) at high latitudes in both the stratosphere and upper troposphere (with positive wave driving anomalies in the lower troposphere). The PV tendency cross-section (Fig. 7c) reveals a consistent pattern of PV decreases (increases) at high (mid) latitudes in both the stratosphere and troposphere. Additional spectral analyses reveal that the EP flux and wave driving patterns are predominantly due to large-scale low frequency eddies (time scales greater than 10 days, Fig. 7e). Thus, the SD period is associated with an anomalous upward flux of planetary wave activity emanating from the lower troposphere.

It is evident that the anomalous wave driving is locally of sufficient magnitude to account for a considerable portion of the zonal wind tendency pattern in Fig. 7a. However, we do not expect

a precise quantitative correspondence between the two fields since (a) the net zonal wind response to the wave forcing will be vertically spread via the residual mean meridional circulation (as discussed in Section 2) and (b) frictional dissipation (third term in equation 1) will tend to partially offset the effects of wave driving. Nonetheless, it is clear that anomalous wave driving plays a first order role in enacting the observed zonal deceleration pattern.

Since, as discussed above, wave driving anomalies are linked to anomalous meridional eddy PV fluxes, anomalous southward eddy PV fluxes must exist at high latitudes throughout much of the stratosphere and upper troposphere. These eddy fluxes lead to near-polar PV reductions at the same altitudes, consistent with the PV changes observed in Fig. 7c. The remaining question is the relative role of stratospheric and tropospheric PV changes in determining the vertical structure of the observed zonal deceleration pattern (Fig. 7a). This is pursued by applying the piecewise PV tendency inversion procedure outlined in Section 2. The zonal wind tendency pattern induced by stratospheric PV changes is shown in Fig. 7d. As expected, the analysis indicates that stratospheric PV changes account for the vast majority of the zonal deceleration pattern in the high latitude stratosphere. The analysis further suggests that at least a portion of the tropospheric tendency pattern results from the latitudinal redistribution of PV in the stratosphere (most likely the lowermost stratosphere). This makes physical sense given the previously noted inconsistency between the upper tropospheric PV tendency and zonal wind fields as SFW onset approaches. Thus, the tropospheric zonal wind deceleration pattern during the SD period is due in part to a direct response to attendant latitudinal PV redistributions occurring in the lower stratosphere.

We present the same diagnostic analyses for the TD period (Days +5 to +10) in Fig. 8. As discussed earlier, this period is characterized by opposing tropospheric deceleration and

stratospheric acceleration features, both of which are evident in Fig. 8a. The associated anomalous EP flux and wave driving patterns are more complex, however, than for the SD period. Focusing on the high latitude region of interest we observe anomalous downward EP fluxes extending through much of the stratosphere to the tropopause. At tropospheric altitudes the EP flux anomaly pattern is very weak north of 70°N (the region of interest). This high latitude EP flux anomaly pattern is associated with positive wave driving anomalies throughout the stratosphere and negative wave driving anomalies in the upper troposphere. The wave driving pattern (again dominated by low frequency eddies, Fig. 8e) is consistent with the high latitude zonal wind tendency pattern (after accounting for some additional vertical "spreading" of the signal) and the PV tendency pattern (Fig. 8b). But what is the physical mechanism leading to the noted EP flux anomaly pattern at high latitudes?

In discussing Fig. 2 we observed that during the latter stages of the composite SFW evolution the zero line in the total zonal wind field descends into the lowermost stratosphere at high latitudes. Since stationary Rossby waves can't propagate into easterlies, this situation precludes vertical wave propagation into much of the high latitude stratospheric domain. A physical interpretation of Fig. 8b is that, at high latitudes, planetary-scale Rossby wave activity that would normally propagate upward from the Earth's surface into the stratosphere (in a climatological sense) is vertically trapped and absorbed nearby the tropopause leading to the noted anomalous negative wave driving pattern. Meanwhile, at stratospheric altitudes, the anomalous EP flux and wave driving pattern simply reflects the absence of the pattern that would normally exist (again, in a climatological sense) in the presence of weak westerly winds in the high latitude stratosphere. This idea is confirmed in Fig. 8f, which displays the *total* EP flux and wave driving patterns for the TD period. It is evident that there

is little or no wave activity flux present in the stratosphere north of 65°N (in strong contrast to the same analysis for the SD period, Fig. 7f). In particular, there is no net downward flux as one might expect in association with a vertical wave reflection (e.g., Perlwitz and Harnik 2003).

The absence of wave driving also allows the stratosphere to readily relax to climatological conditions, as inferred from Fig. 3. Thus, our results suggest that during the TD period the stratosphere provides an indirect influence upon the high latitude troposphere by vertically trapping tropospheric Rossby wave activity, leading to anomalous zonal decelerations in the upper troposphere at high latitudes. Finally, the piecewise PV tendency inversion analysis suggests that the stratosphere provides little or no direct influence upon the troposphere during TD (noting that the difference between Fig. 8a and 8d represents the zonal wind tendencies induced by tropospheric PV changes). If anything, the troposphere acts to partly offset the influence of stratospheric PV tendencies upon the circulation of the lowermost stratosphere (compare Figs. 8a and 8d).

We conclude that during the SD and TD periods the stratosphere provides respective direct and indirect dynamical influences upon the annular tropospheric circulation. Of course, it is critical to emphasis that in both cases the stratosphere-troposphere dynamical coupling is mediated by upward propagating tropospheric planetary waves. In the absence of such waves the stratospheric dynamical changes would be eliminated. Consequently, we consider these downward dynamical influences as feedback mechanisms in an intrinsically coupled dynamical system comprised of tropospheric and stratospheric parts.

5. Summary

We have performed a dynamically-oriented composite study of the evolution of SFW events in order to infer the basic physical mechanisms responsible for the tropospheric zonal decelerations

observed to occur during these events (BMR). Our study begins by characterizing the composite time evolution of the annular circulation at high latitudes during SFW events, which are found to be linked to distinct zonal wind deceleration signatures in the stratosphere and troposphere. Ten days prior to SFW onset (Day -10), circumpolar westerly anomalies are observed over high latitudes in both the troposphere and stratosphere. Between Day -10 and Day 0, the westerly anomaly pattern weakens and is replaced by strong easterly anomalies which first appear in the mid-stratosphere and then strengthen and quickly dive downward through the lower stratosphere into the troposphere at high latitudes. Consequently, this period (denoted SD) exhibits a dramatic and vertically coherent zonal deceleration pattern extending over stratospheric and tropospheric altitudes north of 60^{o}N (with the strongest stratospheric decelerations occurring during this time). Parallel analyses of the total zonal wind field reveal that the westerly winds at mid to high latitudes weaken and retract downward in the lower stratosphere during SD. This results in a lowering of the zero wind line into the high latitude lower stratosphere by Day 0. The early stages of SD are also characterized by a wavenumber one disturbance at stratospheric altitudes, which serves to displace the stratospheric polar vortex away from the North Pole. During SFW onset this disturbance evolves into a circumpolar anticyclonic circulation anomaly.

The high latitude tropospheric easterly anomalies are observed to weaken between Day 0 and Day +5. This is followed by a second period of tropospheric decelerations (denoted TD) between Days +5 and +10 leading to peak amplitudes in the tropospheric easterly anomaly pattern. However, unlike for SD, this period of tropospheric decelerations occurs simultaneously with stratospheric *accelerations* as the large-scale stratospheric circulation relaxes back to climatology. During the TD period there are near-polar increases (decreases) in PV in the stratosphere (upper troposphere).

Zonal-mean dynamical diagnoses were also performed for the two tropospheric deceleration periods. The SD period is characterized by an anomalous upward Eliassen-Palm (E-P) signature at high latitudes extending from the surface to the middle stratosphere. The associated wave driving pattern consists of zonal decelerations extending from the upper troposphere to the mid-stratosphere. The EP flux and wave driving patterns are predominantly due to large-scale low frequency eddies. Thus, during SD an anomalous upward flux of planetary wave activity emanating from the lower troposphere plays a first order role in producing the observed zonal deceleration pattern. Piecewise potential vorticity tendency analyses further indicate that zonal wind decelerations in the lower and middle troposphere result, at least in part, from the direct response to latitudinal redistributions of potential vorticity in the lower stratosphere.

The TD period exhibits opposing tropospheric deceleration and stratospheric acceleration features and a distinct dynamical behavior. During TD there are anomalous *downward* E-P fluxes extending through the high latitude stratosphere but only weak EP flux anomalies in the high latitude troposphere. This EP flux pattern provides positive wave driving anomalies through the high latitude stratosphere and negative wave driving anomalies in the upper troposphere, consistent with the above noted vertical dipole in the zonal acceleration field. The EP flux anomaly pattern in the high latitude stratosphere largely offsets the climatological upward flux leading to general lack of wave activity flux in the high latitude stratosphere. We also note that during this time the zero wind line is located in the lower stratosphere at high latitudes. Considering this dynamical information together, our results suggest that during the TD period the stratosphere indirectly influences the high latitude troposphere by vertically trapping tropospheric Rossby wave activity, leading to anomalous zonal decelerations in the upper troposphere at high latitudes. The tropospheric decelerations that

occur during TD are thereby regarded as a subsequent indirect consequence of SFW events. This situation also permits the stratospheric circulation to readily recover (given the lack of wave driving). We conclude that during SD and TD periods the stratosphere provides direct and indirect dynamical influences, respectively, upon the annular tropospheric circulation. However, we regard these downward influences as feedback mechanisms given the fundamental role of tropospheric Rossby waves in both processes.

Our results suggest both likeness and differences between SFW events and the behavior of SSW events and subseasonal NAM variability. As noted in BMR, there are substantial structural differences between SFW events and the NAM, with SFW circulation anomaly structures retracted northward in comparison with canonical NAM patterns. Compared to the SSW structures studied by Limpasuvan et al. (2004), we find substantial differences in the magnitude and vertical structure of the westerly anomaly pattern observed prior to SFW events. Better correspondence is found with the precursors to the "vortex splitting" events in the recent study of CP. However, we find that the easterly anomaly patterns observed after SFW onset are retracted toward high latitudes compared to the structures identified in both Limpasuvan et al. and CP Finally, we note that the stratospheric wave evolution observed during SFW events closely resembles the case study of "vortex displacement" in CP. This is in contrast to the above-noted correspondence with CP's "vortex splitting" precursors (noting that vortex splitting SSW events are relatively rare during late winter). This dichotomy may simply reflect another basic distinction between SFW and SSW events. Our future work aims to clarify these issues. We also intend to examine the regional tropospheric wave characteristics during SD and TD periods.

Acknowledgments

This paper is based upon a presentation given at the 2006 Chapman Conference on Jets and Annular Structures in Geophysical Fluids in Savannah, Georgia. The study is supported by the NSF Climate and Large-Scale Dynamics Program under Grant ATM-0456157 (under the U.S. CLIVAR Program) and NASA's Living With a Star Targeted Research and Technology Program under Grant NAG5-13492. The NCEP-NCAR reanalyses come from the NOAA Climate Diagnostics Center from their web site at http://www.cdc.noaa.gov/.

References

Andrews, D. G., J. R. Holton, and C. B. Leovy, 1987: *Middle atmosphere dynamics*. Academic Press, 489 pp.

Baldwin, M. P., and T. J. Dunkerton, 2001: Stratospheric harbingers of anomalous weather regimes. *Science*, **294,** 581-584.

Baldwin, M. P., D. B. Stephenson, D. W. J. Thompson, T. J. Dunkerton, A. J. Charlton, and A. O'Neill, 2003: Stratospheric memory and skill of extended-range weather forecasts. *Science,* **301,** 636-640.

Black, R. X., 2002: Stratospheric forcing of surface climate in the Arctic oscillation. *J. Clim.,* **15,** 268-277.

Black, R. X., B. A. McDaniel, and W. A. Robinson, 2006: Stratosphere-Troposphere coupling during spring onset. *J. Climate,* **19,** 4891-4901.

Charlton, A. J., and L.M. Polvani, 2006: A new look at stratospheric sudden warmings. Part I. Climatology and modeling benchmarks, *J. Climate,* **19,** (in press).

Davis, C. A., 1992: Piecewise potential vorticity inversion. *J. Atmos. Sci.,* **49,** 1397-1411.

Edmon, H. J., B. J. Hoskins, and M. E. McIntyre, 1980: Eliassen-Palm cross sections for the troposphere. *J. Atmos. Sci.,* **37,** 2600-2616.

Gillett, N. P., and D. W. J. Thompson, 2003: Simulation of recent Southern Hemisphere climate change. *Science,* **302,** 273-275.

Holton, J. R., 2004: *An introduction to dynamic meteorology. 4th Edition.* Elsevier Academic Press, 535 pp.

Kalnay, E., and Coauthors, 1996: The NCEP/NCAR 40-year reanalysis project. *Bull. Amer. Meteor. Soc.,* **77**, 437-471.

Karpetchko, A., E. Kyro, and B. M. Knudsen, 2005: Arctic and Antarctic polar vortices 1957-2002 as seen from the ERA-40 reanalyses. *J. Geophys. Res.,* **110,** 2005JD006113.

Limpasuvan, V., D. W. J. Thompson, and D. L. Hartmann, 2004: On the life cycle of Northern Hemisphere stratospheric sudden warmings. *J. Climate,* **17,** 2584-2596.

McDaniel, B.A., and R.X. Black, 2005: Intraseasonal dynamical evolution of the Northern Annular Mode. *J. Climate,* **18,** 3820-3839.

Palmer, T.N., 1981: Properties of the Eliassen-Palm flux for planetary scale motions. *J. Atmos. Sci.,* **39,** 992-997.

Perlwitz, J., and N. Harnik 2003: Observational evidence of a stratospheric influence on the troposphere by planetary wave reflection. *J. Clim.,* **16,** 3011-3026.

Thompson, D. W. J., and S. Solomon, 2002: Interpretation of recent Southern Hemisphere climate change. *Science,* **296,** 895-899.

Thompson, D. W. J., and J. M. Wallace, 2000: Annular modes in the extratropical circulation Part I: Month- to-month variability. *J. Climate,* **13,** 1000-1016.

Thompson, D. W. J., and J. M. Wallace, 2001: Regional climate impacts of the Northern Hemisphere annular mode. *Science,* **293,** 85-89.

Thompson, D. W. J., M. P. Baldwin, and S. Solomon, 2005: Stratosphere-Troposphere coupling in the Southern Hemisphere. *J. Atmos. Sci.,* **62,** 708-747.

Waugh, D. W., W. J. Randel, S. Pawson, P. A. Newman, E. R. Nash, 1999. Persistence of the lower stratospheric polar vortices, *J. Geophys. Res.*, **104,** 27191-27202.

Waugh, D. W., and P. P. Rong, 2002: Interannual variability in the decay of lower stratospheric Arctic vortices. *J. Meteor. Soc. Japan,* **80,** 997-1012**.**

Figure Legends

Figure 1. Composite time evolution of the zonally-averaged zonal wind anomalies for lags **(a)** -15, **(b)** -10, **(c)** -5, **(d)** 0, **(e)** +5, and **(f)** +10 relative to SFW onset. Units are m s^{-1}. The blue and yellow contour lines indicate the 90 and 95% confidence levels for a 2-sided t-test. The quasi-horizontal purple line indicates the approximate climatological position of the tropopause.

Figure 2. Composite time evolution of the zonally-averaged zonal wind for lags **(a)** -15, **(b)** -10, **(c)** -5, **(d)** 0, **(e)** +5, and **(f)** +10 relative to SFW onset. Units are m s^{-11}.

Figure 3. Composite time evolution of the zonally averaged zonal wind field. Figure **(a)** shows the zonal wind anomalies averaged from 70N to 80N. The blue and yellow contour lines indicate the 90 and 95% confidence intervals for a 2-sided t-test. Figure **(b)** shows the total wind field averaged from 70N to 80N. Units in both figures are m s^{-1}.

Figure 4. Composite time evolution of the 50 hPa geopotential heights for lags **(a)** -15, **(b)** -10, **(c)** -5, **(d)** 0, **(e)** +5, and **(f)** +10 relative to SFW onset. Contour interval is 50 m.

Figure 5. Composite time evolution of the low-pass filtered 50 hPa potential vorticity anomalies for lags **(a)** -15, **(b)** -10, **(c)** -5, **(d)** 0, **(e)** +5, and **(f)** +10 relative to SFW onset. Units are 10^{-6} s^{-1}.

Figure 6. Composite time evolution of the zonally averaged potential vorticity anomaly field at high latitudes. Figure **(a)** shows the low-pass filtered PV anomalies averaged from 80N to 90N. Units are 10^{-6} s^{-1} Figure **(b)** shows the time-tendency of the low-pass filtered PV anomalies averaged from 80N to 90N. Units are 10^{-6} s^{-1} day^{-1}. See text for details on the temporal filtering

Figure 7. Zonal-mean diagnoses averaged over lags -10 to 0 relative to SFW onset. **(a)** zonal wind anomaly tendency (units of m s^{-1} day^{-1}), **(b)** anomalous EP-flux vectors (units m^3 s^{-2}) and wave driving (units of m s^{-1} day^{-1}), **(c)** changes in the zonally averaged PV field (units of 10^{-6} s^{-1}), **(d)** the zonal wind tendency due to stratospheric PV anomaly changes (units of m s^{-1} day^{-1}) , **(e)** as in figure **(b)** but for the low-pass eddies and **(f)** the total EP-flux and wave driving fields. EP-flux vectors are scaled to point in the proper direction while enhancing magnitudes at successively higher altitudes to facilitate visibility (see McDaniel and Black 2005 for a detailed discussion of this plotting convention)..

Figure 8. As in Fig. 7 except averaged over lags +5 to +10 relative to SFW onset.

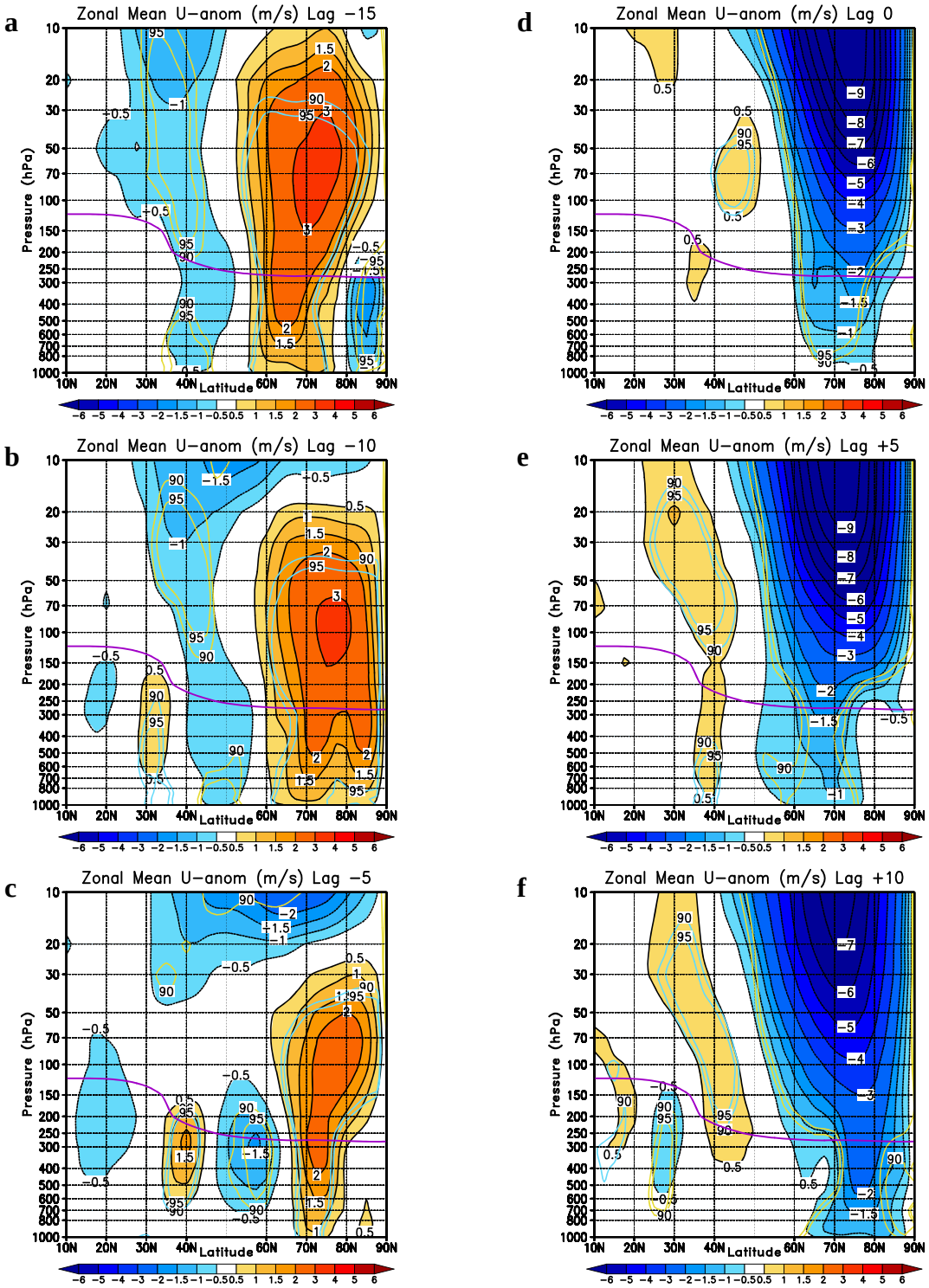

Figure 1

Composite time evolution of the zonally-averaged zonal wind anomalies for lags **(a)** -15, **(b)** -10, **(c)** -5, **(d)** 0, **(e)** +5, and **(f)** +10 relative to SFW onset. Units are m s^{-1}. The blue and yellow contour lines indicate the 90 and 95% confidence levels for a 2-sided t-test. The quasi-horizontal purple line indicates the approximate climatological position of the tropopause.

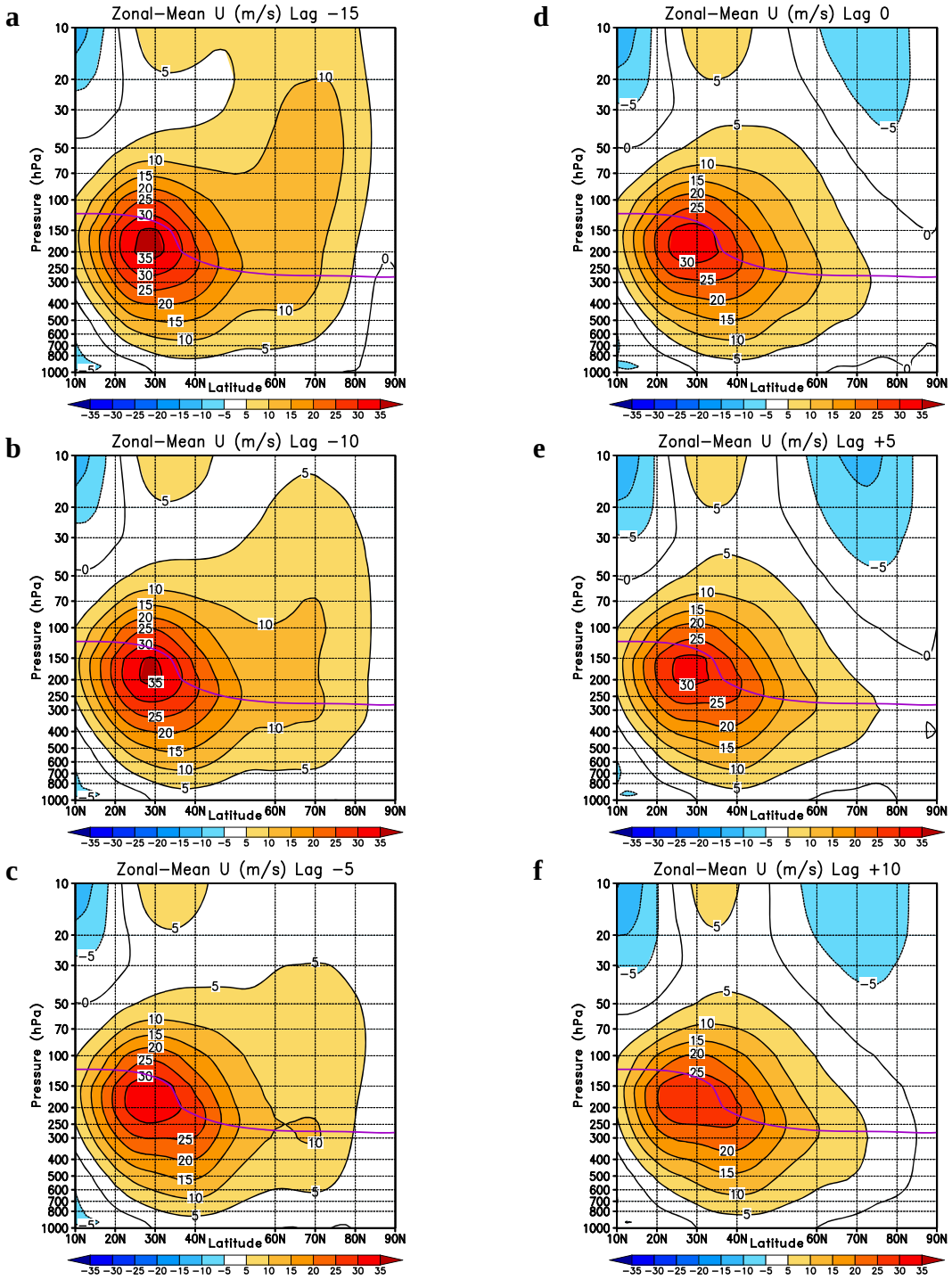

Figure 2

Composite time evolution of the zonally-averaged zonal wind for lags **(a)** -15, **(b)** -10, **(c)** -5, **(d)** 0, **(e)** +5, and **(f)** +10 relative to SFW onset. Units are m s^{-1}.

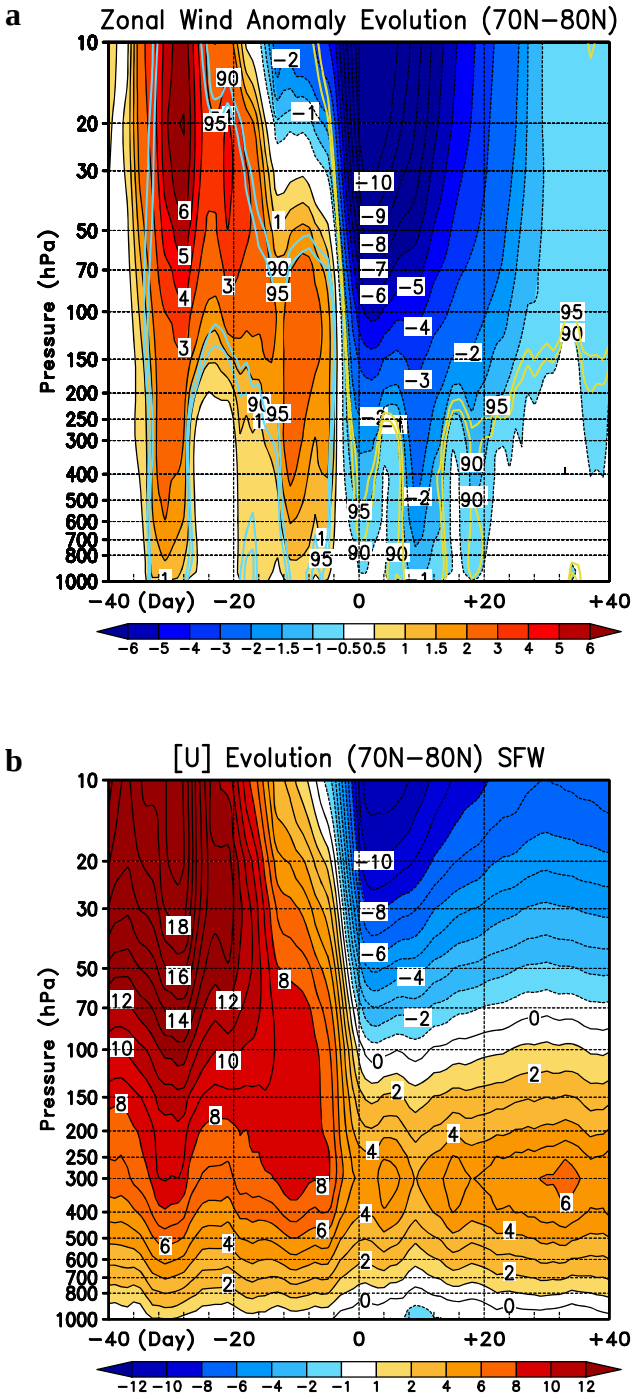

Figure 3

Composite time evolution of the zonally averaged zonal wind field. Figure **(a)** shows the zonal wind anomalies averaged from 70N to 80N. The blue and yellow contour lines indicate the 90 and 95% confidence intervals for a 2-sided t-test. Figure **(b)** shows the total wind field averaged from 70N to 80N. Units in both figures are m s^{-1}.

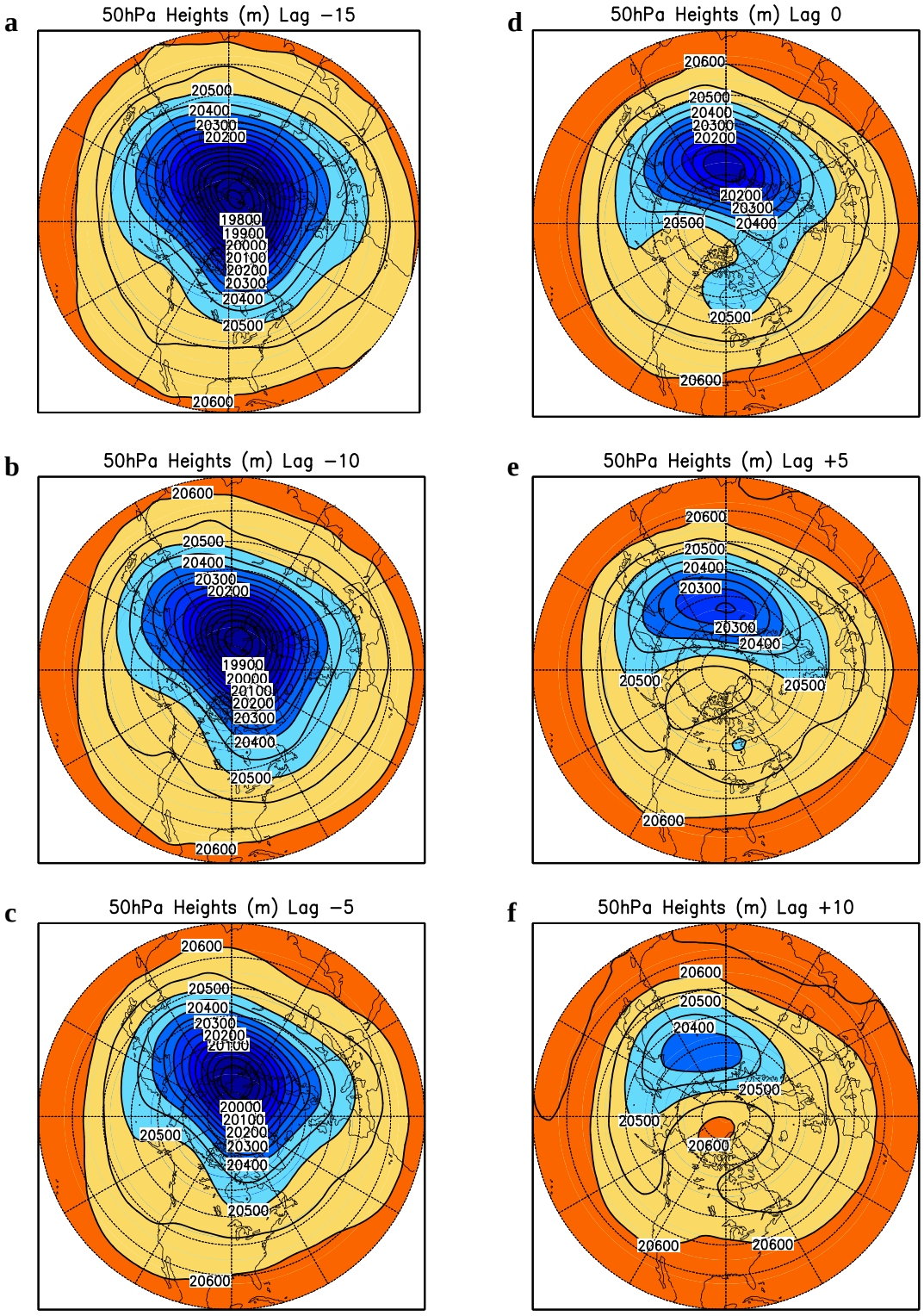

Figure 4

Composite time evolution of the 50 hPa geopotential heights for lags **(a)** -15, **(b)** -10, **(c)** -5, **(d)** 0, **(e)** +5, and **(f)** +10 relative to SFW onset. Contour interval is 50 m.

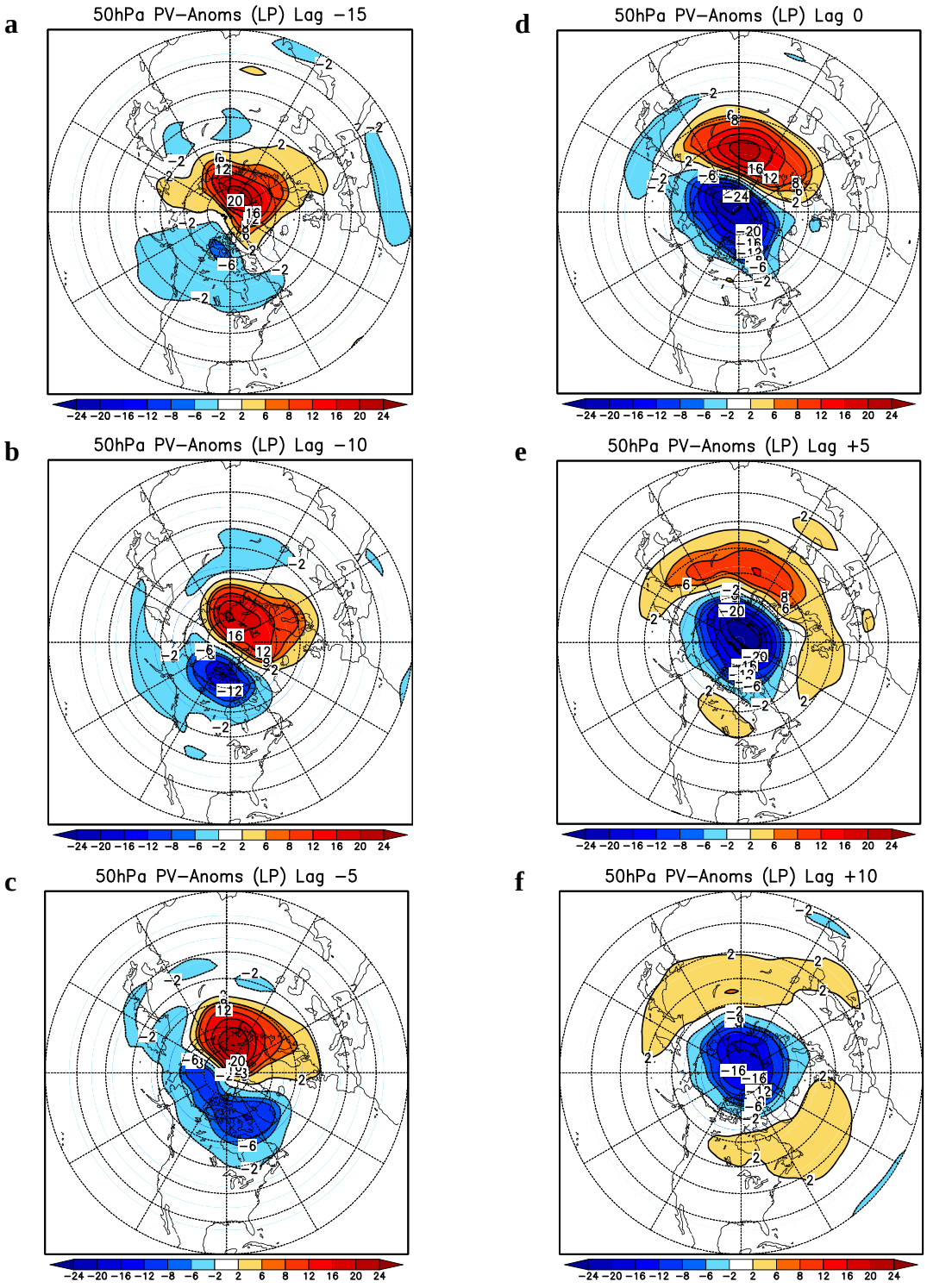

Figure 5

Composite time evolution of the low-pass filtered 50 hPa potential vorticity anomalies for lags **(a)** -15, **(b)** -10, **(c)** -5, **(d)** 0, **(e)** +5, and **(f)** +10 relative to SFW onset. Units are 10^{-6} s^{-1}.

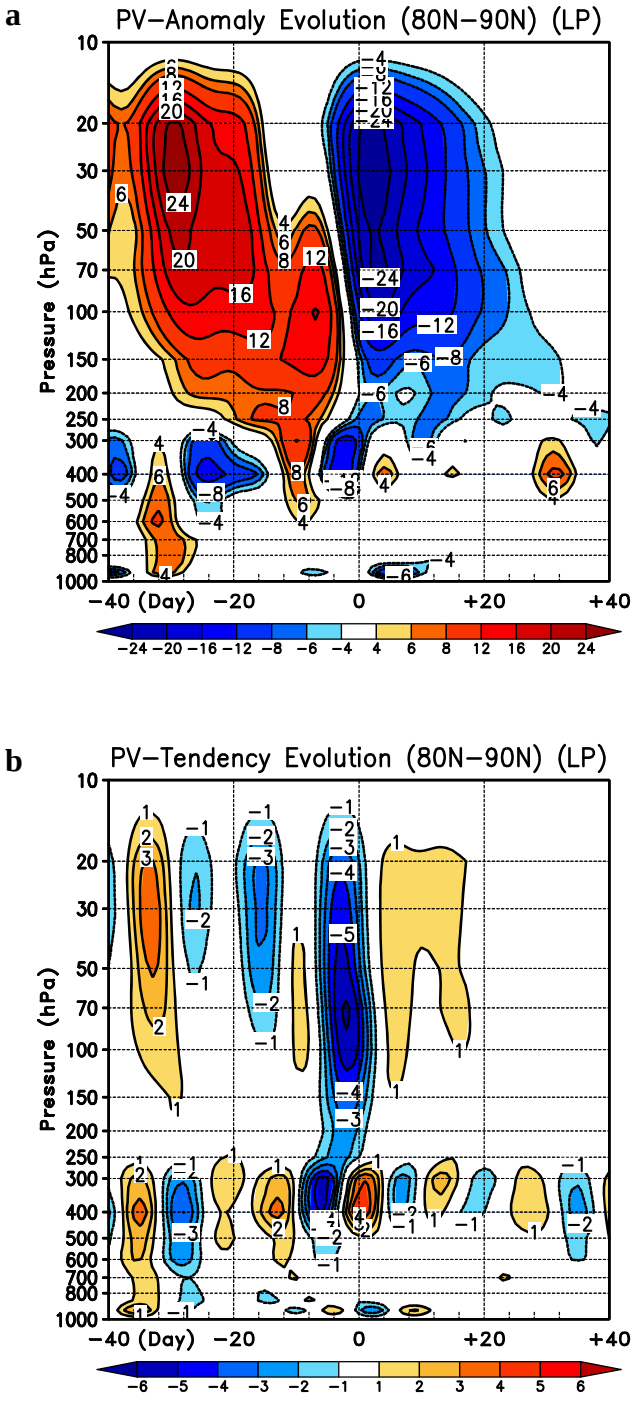

Figure 6

Composite time evolution of the zonally averaged potential vorticity anomaly field at high latitudes. Figure **(a)** shows the low-pass filtered PV anomalies averaged from 80N to 90N. Units are 10^{-6} s^{-1} Figure **(b)** shows the time-tendency of the low-pass filtered PV anomalies averaged from 80N to 90N. Units are 10^{-6} s^{-1} day^{-1}. See text for details on the temporal filtering.

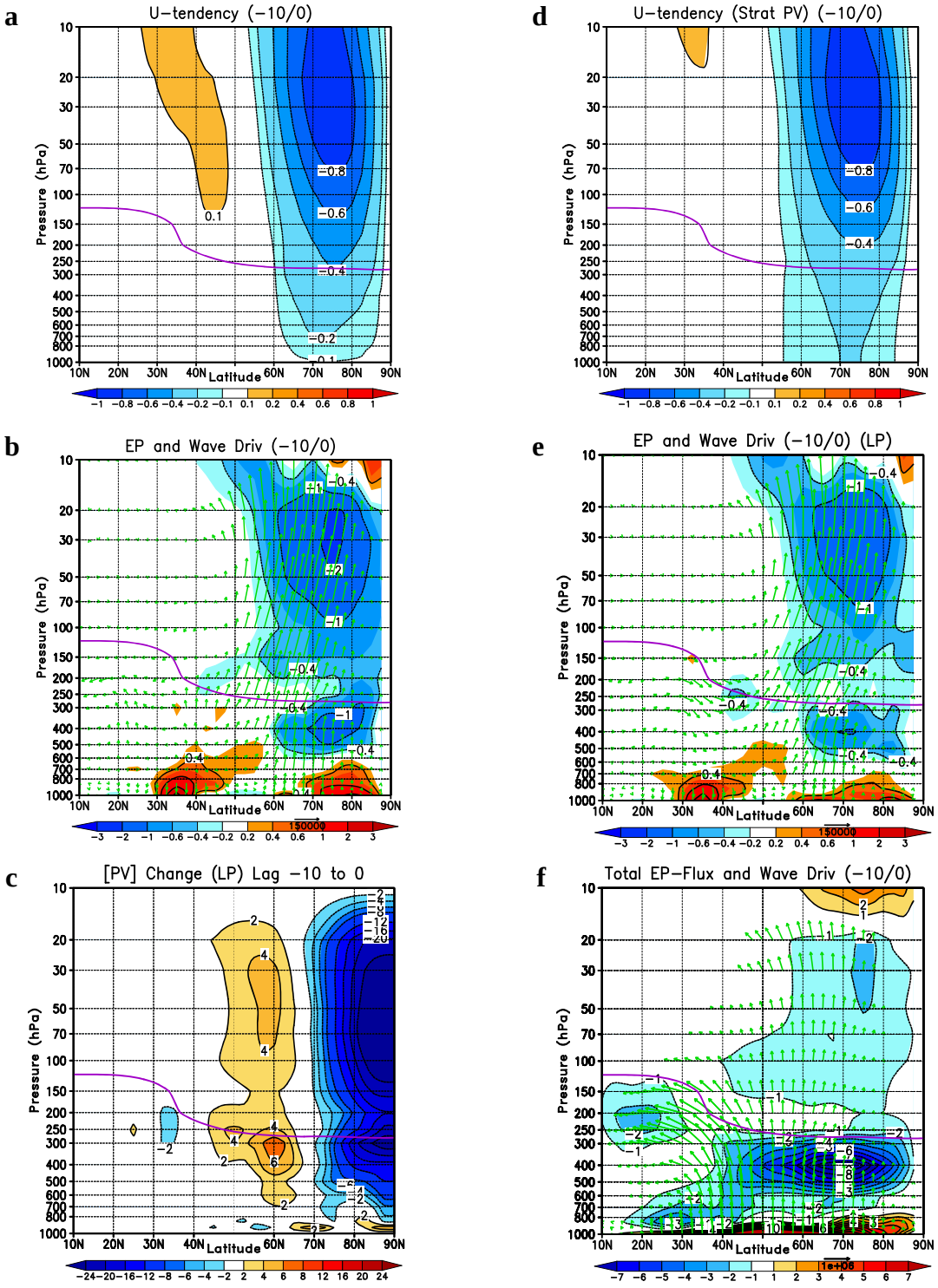

Figure 7

Zonal-mean diagnoses averaged over lags -10 to 0 relative to SFW onset. **(a)** zonal wind anomaly tendency (units of m s^{-1} day^{-1}), **(b)** anomalous EP-flux vectors (units m^3 s^{-2}) and wave driving (units of m s^{-1} day^{-1}), **(c)** changes in the zonally averaged PV field (units of 10^{-6} s^{-1}), **(d)** the zonal wind tendency due to stratospheric PV anomaly changes (units of m s^{-1} day^{-1}) , **(e)** as in figure **(b)** but for the low-pass eddies and **(f)** the total EP-flux and wave driving fields. EP-flux vectors are scaled to point in the proper direction while enhancing magnitudes at successively higher altitudes to facilitate visibility (see McDaniel and Black 2005 for a detailed discussion of this plotting convention).

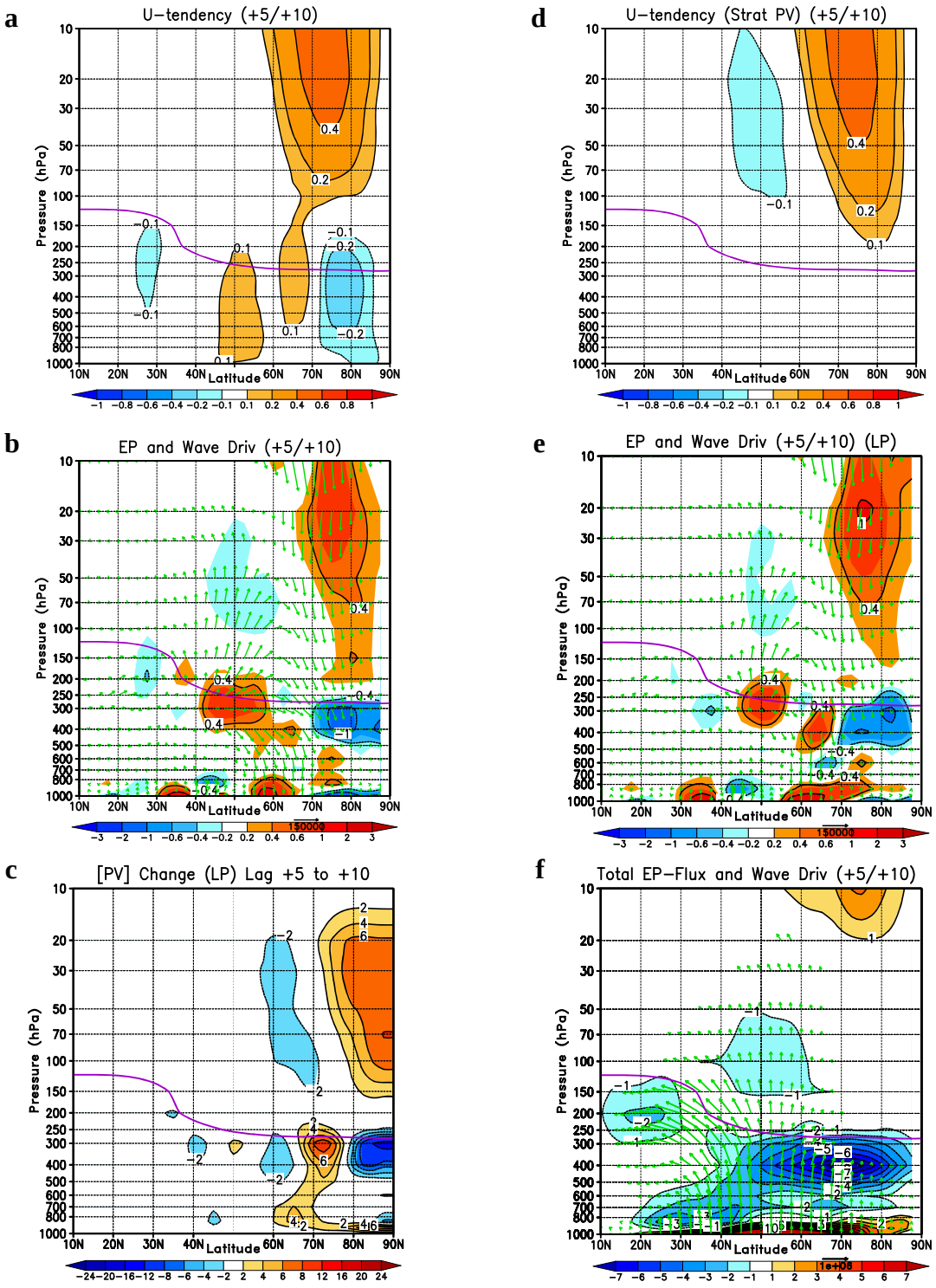

Figure 8

As in Fig. 7 except averaged over lags +5 to +10 relative to SFW onset.